Potentiometric CheqSol and Standardized Shake-Flask Solubility Methods are Complimentary Tools in Physicochemical Profiling

Diego Lucero-Borja[1], Xavier Subirats[1], Rafael Barbas[2], Rafel Prohens[2], Alex Avdeef[3], Clara Ràfols[1,*]

[1] Institute of Biomedicine (IBUB) and Department of Chemical Engineering and Analytical Chemistry, Universitat de Barcelona, Martí i Franquès 1-11, 08028 Barcelona, Spain

[2] Unitat de Polimorfisme i Calorimetria, Centres Científics i Tecnològics, Universitat de Barcelona, Baldiri Reixac 10, 08028 Barcelona, Spain

[3] in-ADME Research, 1732 First Avenue #102, New York, NY 10128, USA

[*] Corresponding author

Diego Lucero-Borja: dslucerob@ub.edu

Xavier Subirats: xavier.subirats@ub.edu

Rafael Barbas: rafa@ccit.ub.edu

Rafel Prohens: rafel@ccit.ub.edu

Alex Avdeef: alex@in-adme.com

Clara Ràfols: crafols@ub.edu

Phone: +34 934 021 284, Fax: +34 934 021 233

Abstract

The solubility of three drugs (glimepiride, pioglitazone, sibutramine) with different acid/base properties and expected supersaturation behavior was examined in detail using the shake-flask (SF) and potentiometric (CheqSol) methods. Both uncharged (free) species and hydrochloride salts were used as starting materials. On the one hand, the SF method provided information about the thermodynamic solubility at any pH value, including the counterion-dependent solubility of ionic species. Additionally, this method easily allowed the identification of the solid phase in equilibrated solutions by powder X-ray diffraction, and the detection and quantification of aggregation and complexation reactions. On the other hand, CheqSol method permitted the measurement of the equilibrium solubility of neutral species, the observation of changes in solid forms, and the extent and duration of supersaturation (kinetic solubility) for "chaser" compounds. The combined information from both methods gave an accurate picture of the solubility behavior of the studied drugs.

Keywords

CheqSol; Supersaturation; Shake-flask; Salts; Thermodynamic solubility; Solubility-pH profile

1. Introduction

Solubility is a fundamental physicochemical property affecting the bioavailability of potential drug candidates, especially those intended for oral administration. Together with permeability, solubility is used in the Biopharmaceutics Classification System (BCS) to describe the behavior of a drug (Amidon et al., 1995). Several methods are available for the determination of solubility, which might be especially convenient at different stages of the drug discovery process (Avdeef, 2012; Di et al., 2012; Veseli et al., 2019). For instance, high-throughput methods based on DMSO solutions of drug added to aqueous buffer, followed by light scattering/turbidity or UV plate reader detection systems are adequate for early stages, but more accurate (and low-throughput) approaches are required for late stage discovery candidates. Among these latter ones, the shake-flask (SF) method is the "gold standard". Sample is added into a flask and dissolved in an aqueous buffer until the presence of an excess solid. Then the flask is shaken (or stirred) for a long time allowing equilibration between solid and saturated solution. According to the recommendations of regulatory agencies (EMA, 2018; FDA, 2017), several pH conditions should be evaluated in order to define the pH-solubility profile of the drug within range of 1-6.8, corresponding to the pH variations in the upper gastrointestinal tract. These guidelines also foresee alternative methods with proven ability to predict the equilibrium solubility of the test drug substance, such as the CheqSol potentiometric titration method (Box et al., 2006; Stuart and Box, 2005).

In the CheqSol method the sample is completely dissolved at a certain pH in order to ensure the compound in its more soluble charged species (acidic medium for bases, BH^+; alkaline for acids, A^-). Then the solution is titrated with strong base or acid until a first precipitate is induced and optically detected, followed by alternate back-titration cycles between fully dissolved and precipitating solutions, which finally allows the calculation of solubility from mass and charge balances, and pH measurements (Box et al., 2009).

The present study is focused on the accurate characterization by SF and CheqSol methods of the solubility behavior of three different drugs (glimepiride, pioglitazone, and sibutramine) and the effect of the starting solid (free species or salt). In fact, both procedures not only provide information about the thermodynamic solubility of the neutral compound (intrinsic solubility), but also on different features relevant for understanding the solubility process of the drug (Table 1). From the measured pH and the added titrant volumes, the potentiometric method calculates the concentration of the drug in solution. The method can estimate the extent and duration of supersaturation, which might be very relevant parameters for the bioavailability of an orally administered drug beyond its thermodynamic solubility. The SF method easily allows the collection of the precipitate after phase separation, and thus the identification by powder X-ray diffraction (PXRD) of the solid in equilibrium at a particular pH value. This is especially relevant because the particular form of the solid, which

plays a key role in the solubility of active pharmaceutical ingredient, clearly depends on the pH (precipitation of uncharged "free" species or salt comprising the drug) and ionized forms on the counterions present in the buffered solution.

The three studied drugs show different acid-base behavior. Glimepiride, pioglitazone and sibutramine are, respectively, an acid, an ampholyte and a base, each expected to show distinctive solubility-pH profiles. Two different computer programs, ACD/Labs (Advanced Chemistry Development, Canada) and *p*DISOL-X (in-ADME Research, USA), were used to predict these profiles from the molecular structure of the compounds, and the results are presented in Figure 1. Similar plots were obtained for glimepiride, but differences in solubility were clear for pioglitazone, and a difference of 1 unit was observed for the predicted pK_a of sibutramine depending on the program used. In addition to their ionization features, these drugs have different molecular properties and therapeutic indications or mechanisms of action. Sibutramine was used for the treatment of obesity until 2010. It is the smallest of the three studied drugs, showing poor hydrogen-bonding capabilities and a highly reduced polar surface area. In contrast, glimepiride is a polar antidiabetic drug with a sum of 12 hydrogen-bond acceptors/donors and a molecular weight of nearly 500. The antidiabetic pioglitazone exhibits molecular properties in between of sibutramine and glimepiride, with the exception of a relative high contribution of polar atoms and their attached hydrogens (Table 2 and Fig. 1). Since supersaturation in aqueous solution is expected for molecules with high polar surface and a sum of at least three hydrogen-bond donors and acceptors (Box et al., 2009), it is of interest to study this property for glimepiride and pioglitazone using the CheqSol method. On the contrary, the base sibutramine is not expected to show a significant supersaturation.

2. Material and methods

2.1. Chemicals and reagents

Glimepiride (> 99%), pioglitazone (> 99%), sibutramine (> 99%) and the hydrochloride salt of pioglitazone and sibutramine (> 99%) were provided by the Polymorphism and Calorimetry Unit of the Scientific and Technological Centers of University of Barcelona (CCiT-UB). Acetic acid (> 99%), trifluoroacetic acid (min 99.0%), dimethylsulfoxide (> 99%), hydrochloric acid 1 M Titrisol, sodium hydroxide 1 M Titrisol, potassium hydroxide 1 M Titrisol, and methanol (HPLC gradient grade) were from Merck (Darmstad, Germany). Ethylenediamine (min 98.8%), potassium chloride (> 99%), formic acid (min 98%) and phosphoric acid (85% in water) were from Sigma-Aldrich (St. Louis, MO, USA).

2.2. Instruments

pK_a and potentiometric intrinsic solubility assays were performed using the GLpK_a and PCA 200 titrators from Sirius Analytical Instruments Ltd. (Forest Row, UK). Both instruments include a D-PAS probe, a bifurcated fibre-optic dip probe from Hellma Analytics (Müllheim, Germany) with path length of 1 cm, and a two channels solvent degasser from SMI-LabHut Ltd. (Churcham, UK). The operation of the apparatus was controlled by a personal computer running the Refinment Pro 2 and the CheqSol software.

SF experiments were performed using a Movil-ROD rotation shaker from Selecta (Abrera, Spain) in closed test tubes at 25 ºC. pH was measured using a Crison 5014 combined electrode connected to a GLP 22 potentiometer from Crison (Alella, Spain) calibrated with standard aqueous solutions (pH 7.00 and 4.01 or 9.21). After equilibration, phases were separated using a Rotanta 460RS centrifuge from Hettich Lab Technologies (Tuttingen, Germany) for 30 min at 3500 rpm and 25 ºC. Solubility was quantified by liquid chromatography using a Shimadzu Nexera UPLC system with two LC-30AD pumps, a DGU-20A5 online degasser, a SIL-30AC autosampler, a SPD-M20A diode array detector, a CTO-10ASvp oven at 25 ºC, and a CBM-20Alite controller. A 1.7 µm, 50 x 2.1 mm Waters (Milford, MA, USA) Acquity BEH C18, 50 mm x 2.1 mm column was employed, at a flow rate of 0.5 mL min^{-1} and injection volume of 0.2 µL. Mobile phases consisted of methanol and aqueous 0.1 M formic acid pH 3.0.

Powder X-ray diffraction characterization was performed using a PANalytical X'Pert PRO MPD θ/θ diffractometer of 240 millimetres of radius in transmission configuration using Cu Kα1+2 radiation (λ = 1.5406 Å) with a focusing elliptic mirror and a PIXcel detector working at a maximum detector's active length of 3.347°. Configuration of convergent beam with a focalizing mirror and a transmission geometry with flat sample sandwiched between low absorbing films measuring from 1 to 40° in 2θ, with a step size of 0.026° and measuring times of 75 or 300 seconds per step.

Differential scanning calorimetry analysis was carried out by means of a Mettler-Toledo DSC-822e calorimeter. Experimental conditions: aluminium crucibles of 40 µL volume, atmosphere of dry nitrogen with 50 mL/min flow rate, heating rate of 10ºC/min. The calorimeter was calibrated with indium of 99.99% purity.

Thermogravimetric analysis was performed on a Mettler-Toledo TGA-851e thermobalance. Experimental conditions: alumina crucibles of 70 µL volume, atmosphere of dry nitrogen with 50 mL/min flow rate, heating rate of 10ºC/min.

2.3. pK_a determination by spectrophotometric method

Due to the very low solubility of the studied compounds, pK_a values were spectrophotometrically determined using the methodology described in the current literature (Tam

and Takács-Novák, 2001). Briefly, 30 or 40 µL of stock solution (10 mM of compound in DMSO) and 250 µL of a 15 mM potassium phosphate buffer were added to 10 mL of a 0.15 M KCl ionic strength adjusted (ISA) aqueous solution. The pH of the sample was initially selected to titrate from low to high pH for basic compounds and high to low pH for acidic ones to avoid precipitation. Titrants were 0.5 M potassium hydroxide and 0.5 M hydrochloric acid. When the compound was not soluble enough in water, pK_a was determined in different methanol/water mixtures and the aqueous pK_a was obtained by extrapolation using Yasuda-Shedlovsky equation (Avdeef et al., 1993). All measurements were performed at least in triplicate at 25 ± 0.1 ºC under nitrogen atmosphere. The collected data was refined through the Refinement Pro 2 software and the pK_a values were obtained by target factor analysis (Tam and Takács-Novák, 2001).

2.4. Solubility determination by CheqSol method

Suitable amounts of sample (between 5 and 40 mg) were accurately weighed into the titration vessel and 10 mL of ISA solution were added. The pH value was adjusted with the suitable titrant (0.5 M hydrochloric acid or 0.5 M potassium hydroxide) to a value where the sample was fully ionized and thus completely dissolved. Then, samples were automatically back titrated until precipitation was induced, followed by the alternate cycles of subsaturation and supersaturation. Intrinsic solubility was determined from the pH in the chasing equilibrium points (*cheqpoints*) where equilibrium was reached as described elsewhere (Stuart and Box, 2005). All measurements were performed at least in quadruplicate at 25 ± 0.1 ºC under argon atmosphere.

2.5. Solubility determination by shake-flask method

The recommended (Avdeef et al., 2016) *Mass Spectrometry-Friendly Minimalist Universal Buffer* (MS-MUB), consisting of 25 mM acetic acid, 25 mM ethylenediamine, and 75 mM trifluoroacetic acid (TFA), was used to prepare buffers between pH 1.8 and 12.0 for the determination of solubility-pH profiles. The desirable pH was adjusted by 0.5 M NaOH or 0.5 M HCl. The average buffer capacity and ionic strength of the pH buffers were 8.3mM/pH and 0.096M, respectively (in the absence of added sample). At each pH buffer, at least three aliquots were prepared by adding enough solid sample to obtain a saturated solution in 3 mL of the buffer solution. The incubation was carried out at controlled temperature (25 ± 0.1 ºC) for 48 h (24 h stirring and 24 h sedimentation). The pH was measured after 4h of stirring and readjusted if necessary with sodium hydroxide or hydrochloric acid, and finally the pH was measured again before the phase separation by centrifugation. The concentration of sample in the supernatant was determined by liquid chromatography, whereas the solid was vacuum filtered and dried for at least 30 min to determine its crystal form by PXRD.

2.6. Refinement of intrinsic and salt solubility and aggregation constants

The SF solubility data analysis method uses log *S* - pH as measured input data (along with the standard deviations in log *S*) for the *p*DISOL-X computer program, as described previously (Avdeef, 2018; Marković et al., 2019; Völgyi et al., 2013). Briefly, an algorithm was developed which considers the contributions of all species present in solution, including all components of buffers or mixtures thereof. The approach does not assume that the traditional Henderson-Hasselbalch equations are valid. The computational algorithm derives its own implicit equations internally, given any practical number of equilibria and estimated constants. The constants can be subsequently refined by weighted nonlinear least-squares regression. Drug-salt precipitates, -aggregates, -complexes, -bile salt and -surfactant (Avdeef, 2018) species can be modeled. The presence of specific drug-buffer (Marković et al., 2019) species can be tested. The computer program calculates the distribution of species corresponding to a sequence of additions of acid titrant (e.g., HCl, or ionizable titrants, such as H_3PO_4) to simulate the speciation in the suspension down to pH ~ 0. Subsequently, a sequence of perturbations with a strong base (e.g., NaOH) is simulated, with the solubility calculated at each point (in pH steps of 0.005-0.2), up to pH ~ 13. The ionic strength is rigorously calculated at each step, and pK_a values (as well as solubility products, aggregation constants) are accordingly adjusted. At the end of the speciation simulation, the calculated log *S* vs. pH curve is compared to measured log *S* vs. pH. A log *S*-weighted nonlinear least squares procedure refines the proposed equilibrium model, using analytical expressions for the differential equations. The process is repeated until the differences between calculated and measured log *S* values reach a minimum.

3. Results and discussion

3.1. Solubility by CheqSol method

In order to determine the intrinsic solubility (S_0) of the studied drugs by the potentiometric method, it was first necessary to measure accurately the corresponding pK_a values (section 2.3). The determined acidity constants are reported in Table 3.

For the base sibutramine and the ampholyte pioglitazone two different starting solids were considered in the solubility experiments, the free neutral species and their hydrochloride salts (in the case of glimepiride, because of its acidic nature, only the free acid was assayed). No significant differences were found in the measured intrinsic solubility (S_0, that of the neutral species) of each compounds depending on the particular solid form initially weighed, which is not unexpected provided that the CheqSol method involves the complete dissolution in the ionized form before the beginning of the titration procedure. Determined intrinsic solubilities are reported in Table 3, and in the cases of glimepiride and pioglitazone they are consistent with literature values also potentiometrically determined.

In addition to the thermodynamic solubility of the neutral species (S_0) and in contrast to SF method, CheqSol provides valuable information about supersaturation of the studied molecules (Box et al., 2009). Figure 2 shows the *Bjerrum Curves* (Avdeef, 1998) (left panels) and the neutral species concentration-time profiles along time course (right panels) for the three drugs. The Bjerrum plots show the theoretically expected changes in the protonation state (molecular charge) caused by ionization in absence (solution curve) or in presence of precipitation, together with experimental data points. In the beginning of glimepiride and pioglitazone titrations (left panels in Figs. 2A and 2B), starting at basic pH, the measured data follow the *solution Bjerrum curve*. Due to supersaturation this solution curve is followed beyond the pH needed to start precipitation (crossing of *solution* and *precipitation curves*), and when the solid starts precipitating the data points come closer to the *precipitation curve*. Finally, the chasing equilibrium around the *precipitation curve* takes place, consisting of flips between induced supersaturated and subsaturated states by alternate additions of acidic and basic titrant. Thus, both glimepiride and pioglitazone show a *chaser* behavior, and the variations on the concentration of the neutral species during the analysis time provide information about the supersaturation extent and time (right panels in Figs. 2A and 2B). The supersaturation ratio (R_s) for glimepiride, determined as the ratio of maximum calculated concentration of neutral specie and S_0, is about 125 and the duration of this supersaturation state (t_{sat}) is about 6 min (Table 3).

Since pioglitazone is an amphoteric molecule the titration could be started either in strong acidic (drug in H_2X^+ form) or in alkaline medium (X^-). However, the complete dissolution of the compound was not achieved at pH 1.8, and thus all titrations were started at pH 11.5. Similar supersaturation times were found for glimepiride and pioglitazone, but with a lower supersaturation ratio (Table 3). This is consistent with the lower hydrogen-bonding capabilities and the lower polar surface of pioglitazone compared to glimepiride (Table 2). However, in contrast to glimepiride, the concentration profile of the neutral species shows for pioglitazone (Fig 2B, right panel) after about 2 h a rise of the chasing equilibrium points, probably as a consequence of a solid form change into a more soluble one.

Interestingly, the *Bjerrum curves* for sibutramine (Fig. 2C) clearly shows two different behaviors. First, as a *non-chaser*, the compound does not form a supersaturated solution and the experimental points follow the *precipitation Bjerrum curve*. However, at around pH 7.1–7.6 sibutramine switches to a *chaser* behavior (with supersaturation). The change from *non-chaser* to *chaser* can be also monitored in the neutral species concentration-time profile: about 60 min after the beginning of the experiment there is an increment in the concentration of the neutral species in solution, followed by a sharp concentration drop and the establishment after about 80 min of the chasing equilibrium. The CheqSol software cannot accurately calculate the concentration of neutral species in the section between the concentration drop after the peak and about 80 min (Fig. 2C, right

panel), corresponding to pH values from 10 to 7.6 in the *Bjerrum* graph (left panel), because the molecular charge is close to zero and this affect the algorithms derived from charge and mass balances. After this period of transition a *chaser* behavior is observed. Interestingly, the intrinsic solubility calculated from *cheqpoints* is very similar to that immediately prior to the concentration peak when sibutramine behaved as *non-chaser*. The dual behavior of sibutramine allowed the measurement of intrinsic solubility through the *non-chaser* points using a curve fitting approach to the *precipitation Bjerrum curve*, but also as a *chaser* according to the crossing point method. Similar log S_0 values were obtained in both cases, -5.28 ± 0.06 and -5.37 ± 0.14, respectively (average is presented Table 3).

3.2. Solubility by shake-flask method

3.2.1. Buffer and pH considerations

The solubility-pH profile of each compound was studied by the shake-flask method using the recommended minimalist universal buffer (MS-MUB). This buffering system is expected to provide a reasonable buffer capacity over a wide pH range (2-12) with a nearly constant ionic strength of about 0.1 M, but avoiding the introduction of salt formers as chloride or phosphate anions (Avdeef et al., 2016). Nevertheless, depending on the nature of the starting solid or the one in equilibrium with the saturated solution (free species or salt) and the solubility of the charged species, the pH of the supernatant medium when equilibration is achieved might significantly differ from the initial pH of buffer (Avdeef et al., 2016; Shoghi et al., 2013). Figure 3 shows the pH variation observed between the pH measured after 4 hours of stirring and the initial pH of the buffer before the addition of the solid. Regarding glimepiride (Fig. 3A), in the acidic pH range, the initial sample and the solid collected was in both cases the neutral species (HA), and therefore a negligible pH variation was observed. When the ionic species (A^-) started to play a relevant role in solution (pH > pK_a) glimepiride took part in the acid-base equilibrium with the buffer, increasing the concentration of protons in solution and thus reducing the pH. However, the scarcely soluble HA still was the solid form in equilibrium, which moderated the pH decrease to only slight variations. However, at pH > 10 the solid phase in equilibrium was no longer the free acid (HA) and the precipitation of the salt (noted as $C^+A^-_{(s)}$ in the Fig. 3A, where C^+ is a buffer component) shifted the equilibrium from HA to A^- releasing H^+ and thus significantly decreasing the solution pH.

When the free pioglitazone (HX) was used only slight variations on pH were found in the equilibration step. At pH lower than pK_{a1} the formation of H_2X^+ consumed H^+ and thus the pH became more basic, and the reversed trend was observed when X^- was involved at pH > pK_{a2} (Fig. 3B). At this point and before discussing the effect on pH of pioglitazone hydrochloride as starting solid, it is needed to mention that only the free species (HX) was found as the solid phase in equilibrium in the

studied pH range. In all experiments the use of the hydrochloride salt of pioglitazone as starting solid (noted as $H_2X^+C^-_{(s)}$ in Fig. 3B) produced a decrease in the solution pH. Two main causes were found to be responsible for the extent of this behavior. The first one was the amount of hydrochloride weighed. Since $HX_{(s)}$ was the only precipitating species, all chloride ions initially introduced with the sample and part of the protons were released in the solution. Consequently, the higher amount of hydrochloride salt, the higher the concentration of chloride in solution and the lower resulting pH. The second cause was related to the buffering capacity of the universal buffer used, which presents local minima at around pH 3, 6, and 9 (Fig. 3B).

The pH variation for sibutramine (free base) was irrelevant in the basic range due to the low solubility of the neutral species, but there was a positive pH variation in acidic conditions because of the protonation of the base in solution ($BH^+_{(aq)}$) and the precipitation of the salt ($BH^+C^-_{(s)}$) (Fig. 3C). Since the salt is quite soluble, the relatively high concentration of protonated base takes over the buffer capacity of MS-MUB resulting in shifts up to 3 pH units. Remarkably, the reversed trend was observed when sibutramine was initially introduced as hydrochloride salt. At pH << pK_a the solid introduced and the precipitating species were of the same nature ($BH^+_{(aq)}$ and $BH^+C^-_{(s)}$) and thus the pH variation was negligible. At about neutral pH the precipitation of the free base ($B_{(s)}$) was induced, reducing the pH as consequence of the deprotonation of $BH^+_{(aq)}$.

3.2.2. Solubility-pH profiles and identification of the collected solids

Calculated solubility-pH profiles, as those shown in Fig. 1, are helpful in planning the experimental setup and measurement conditions of a shake-flask method (interesting pH range, amount of substance needed at each pH, expected concentrations and suitable quantification instruments…), but keeping in mind that estimated values are just an initial approximation.

In this work, intrinsic solubilities (log S_0) and the presence of aggregation reactions were deduced from fittings of experimental solubility data to the most appropriate models (Avdeef, 2007), and only solubilities obtained with the recommended MS-MUB buffer were taken into consideration for this purpose. However, MS-MUB is a complex buffering system and in the particular case of sibutramine several simpler buffers were selected to study the solubility of its salts. Table A.1 in the supplementary material summarizes these solubility data, reporting the measured pH at the end of the sedimentation step (just before the phase separation) and the identification of the solid collected by PXRD (Fig.4).

3.2.2.1 Glimepiride

The solubility-pH profile of glimepiride is presented in Fig. 5. The starting weighed solid was the free acid for the whole studied pH range and it was confirmed by PXRD as the polymorph form

I, the most insoluble one (Bonfilio et al., 2012; Iwata et al., 1997). The diffractograms obtained for the solids collected in the acidic and neutral pH range confirmed the presence of form I, whereas in very alkaline solutions a new solid form was found, which does not correspond to any of the seven crystal forms reported in literature (Grell et al., 1998; Iwata et al., 1997; Tian and Zimmerman, 2017a, 2017b, 2017c, 2017d, 2017e) (Table A.2, Figs. S.1-S.3). Based on the experimental solubility-pH profile in this basic region and the buffer components present in solution, we attribute this solid form to the sodium salt of glimepiride (this cation came from the strong base (NaOH) used to adjust the pH of the MS-MUB buffering system).

Unexpectedly, the fittings of the experimental data to the theoretical Henderson-Hasselbalch equation (Eq. (1)) came to an apparent pK_a for glimepiride that was about 0.5 pH units higher than the potentiometrically measured one, thus suggesting the influence of additional aggregation equilibria. After checking different fitting models, including the formation of neutral, anionic and mixed aggregates, the best fit was obtained when considering the formation a dimeric neutral aggregate of glimepiride ($2\mathrm{HA} \rightleftarrows \mathrm{H_2A_2}$, Eq. (2), case 1a in ref. (Avdeef, 2007)):

$$\log S = \log S_0 + \log(1+10^{\mathrm{pH}-\mathrm{p}K_a}) \quad (1)$$

$$\log S = \log S_0 + \log(1+K_a/[\mathrm{H}^+]+2K_2^{\mathrm{H_2A_2}} S_0) \quad (2)$$

where S_0 is the intrinsic solubility of the monomeric species and $K_2^{\mathrm{H_2A_2}}$ is the formation constant of the aggregate. Since glimepiride molecule has strong and self-complementary hydrogen bond donors and acceptors in its structure, it is plausible that a dimer is formed in solution. In fact, the crystal structure of its polymorphs shows strong self-assembling interactions involving the sulfonamide and urea groups present in the molecular structure (Endo et al., 2003; Gryl et al., 2011; Iwata et al., 1997). Consequently, as shown in Fig. 5, the apparent intrinsic solubility of glimepiride ($\log S_0^{\mathrm{App}}$) is about 0.5 log units higher than log S_0 due to aggregation reactions. The intrinsic solubility for glimepiride reported in this work is consistent with the experimental data measured by Seedher (Seedher and Kanojia, 2009) and Grbic (Grbic et al., 2010) research groups, provided that the aggregation constant of the dimeric neutral species is considered in the solubility model (Table 4). However, aggregation constants differ in more than 1.5 log units, which may indicate supersaturation (equilibration steps of 24 h were reported in the cited papers, but information about sedimentation time after stirring step was not indicated). Additionally, the solubility value of -4.75 measured by Seedher and Kanojia at pH 7.4 using a 0.1 M phosphate buffer (Seedher and Kanojia, 2008) is in good agreement with our results at the same pH value. The lower apparent intrinsic solubility reported by Bergström and coworkers (log S_0 = -7.83 ± 0.10 (Bergström et al., 2007)) contrasts with the ones reported in Table 4, but it should be pointed out that this value was obtained after a double centrifugation process,

which might be prone to a potential sample loss due to adsorption in multiple transfers (Avdeef et al., 2016). Interestingly, the intrinsic solubility determined by the potentiometric approach is about 0.8 units higher, but more similar to the apparent value (log S_0^{App}). A possible explanation might be related to the CheqSol calculation algorithms, which do not foresee deviations from theoretical Hendersson-Hasselbalch equation (Eq. (1)) and consequently the formation of aggregated species in solution. At pH > 8.5 the sodium salt of glimepiride precipitates according to a calculated solubility product constant (pK_{sp}) of 5.35 ± 0.01.

3.2.2.2 Pioglitazone

In the case of pioglitazone, the solid collected in the studied pH range (2-11) was in all cases the neutral species, independently whether the starting material was the free form or its hydrochloride salt, and its solubility-pH profile (Fig. 6) clearly matched the model for an amphoteric (non-zwitterionic) compound with aggregation (apparently elevated solubility in the mid-pH region) (Avdeef, 2007):

$$\log S = \log S_0 + \log(1 + K_{a1}/[H^+] + [H^+]/K_{a2} + 2K_2^{H_2X_2} S_0) \quad (3)$$

where K_{a1} and K_{a2} are referred to the basic nitrogen of the pyridine and the acidic proton bound to the nitrogen of the thiazolidinedione group, respectively (Fig. 1 and Table 3). The fitted log S_0 value was -6.98±0.04, about 1 unit lower in comparison to the intrinsic solubility potentiometrically determined in this work (-5.81±0.24), which better matches the apparent intrinsic solubility from the SF analysis (-5.70±0.05). Log $K_2^{H_2X_2}$, with a refined value of 7.98±0.12, corresponds to a dimer formation of the free ampholyte; however, the formation of colloids or nanoparticles could be also responsible for the solubility leveling in this mid-pH region (Gebauer et al., 2014; Irwin et al., 2015). The reported log S_0 by Schönherr using a SiriusT3 instrument lies approximately in the middle of these two values (Table 3). The solubility measured in the present work at pH 7.4 is about 1 log unit lower than that determined by Seedher and Kanojia using a phosphate buffer (Seedher and Kanojia, 2008). However, in a later study (Seedher and Kanojia, 2009) these authors reported the solubility values of pioglitazone in the pH ranges 1.8-3.9 and 7.4-9.5 using glycine based buffers, which allow the calculation of a log S_0 (using Eq. (3) with pK_a values determined in this work) of -6.86±0.16, very consistent with our results. Similarly, Sugita and coworkers (Sugita et al., 2014) cited a solubility-pH profile carried out in the acidic range (1.2-6.8), which permit us to calculate a log S_0 value of -6.63±0.05, again in good agreement with our findings.

3.2.2.3 Sibutramine

The most comprehensive study of this work was performed on sibutramine. Besides the aim of elucidating the effect of the starting material and the precipitating solid, we conducted a systematic research on the solubility of the positively charged species and its relation with the buffer counterions. It was found (Table A.1 and Fig 7A) that the nature of the solid precipitated was independent of the initial solid weighed (free base or hydrochloride salt). Only the neutral form was found at pH values above 5.8, but in more acidic media the solid collected was neither the neutral species nor the hydrochloride salt (Fig. 4). With the aim of identifying this salt, we carried out a series of shake-flask experiments with simple buffers prepared from acetic and trifluoroacetic acid (both constituents of the MS-MUB), but also hydrochloric and phosphoric acids, in order to study the salt formation of their respective anionic conjugate bases with the cationic sibutramine acid. The obtained results are presented in Figs. 7B and 7C. In the acidic pH range, different scenarios were observed: i) When TFA was used as buffering agent, independently of the initial form of sibutramine (free base or hydrochloride salt), the collected solid coincided with that precipitated at acidic media under MS-MUB conditions. This suggests that MS-MUB induces the precipitations of the sibutramine TFA salt in acidic conditions, of which crystalline form was characterized by PXRD, DSC and TGA (Table A.3, Figs. S.4-S.6); ii) In nearly all cases in acidic conditions (with the formerly mentioned exception of TFA), hydrochloride salt was collected from the initially dissolved hydrochloride salt. It must be pointed out that sibutramine·HCl is quite soluble and thus the amount of chloride ions from the weighed sample may very well be higher than the concentration of buffering species in solution; iii) Starting with the free base (in order to minimize the concentration of chloride in solution), a new solid was collected when phosphate buffers were employed (Table A.3, Fig. S.7), attributed to sibutramine phosphate salt; iv) Hydrochloride and phosphate salts of sibutramine were more soluble than those with TFA; v) In the pH region near pH 5.0 (close to the Gibbs pK_a (Avdeef, 1998), *i.e.,* "pH_{max}") the solid phase in equilibrium can be a mixture of the uncharged form of the drug and TFA/phosphate salts. The fitting of the experimental points obtained with the MS-MUB buffer with the formation of TFA salt led to an intrinsic solubility value (log S_0) for sibutramine of -5.62±0.02 , which is near the CheqSol result, and a solubility product constant (pK_{sp}) for the TFA salt of 3.23±0.03 . In a similar approximation, the pK_{sp} for the hydrochloride salt was found to be 2.37±0.01 and thus more soluble than the drug-TFA salt. Interestingly, in the pH range between 8 and 11 a slight positive deviation from the theoretical Hendersson-Hasselbalch behavior is observed (dashed line in Fig. 7), which suggests an interaction between the positively charged ethylenediamine (MS-MUB constituent) and the neutral sibutramine (log $K_{B.enH}$ = 1.54±0.28). The concentration of this aggregate reaches a maximum value at pH 9.4, when the molar fractions of neutral sibutramine (B) and the amphoteric ethylenediamine (enH^+) are expected to be predominant (both about 80% according to

their pK_a values). To the best of our knowledge, there is no solubility data for this drug in the available literature.

4. Conclusions

Shake-flask and CheqSol methods provide accurate, valuable and complementary information about the solubility behavior of compounds with acid-base properties. On the one hand, shake-flask is labor intensive and time consuming, but allows the solubility measurement of free species and their corresponding salts, even in the presence of aggregation or complexation reactions, and the solid precipitated can be easily collected and identified by powder X-ray diffraction. On the other hand, CheqSol is automated and provides additional data on supersaturation, but requires a previous accurate pK_a determination, it is limited to intrinsic solubility (free acid or base) and assumes a Henderson-Hasselbalch behavior.

Potentiometric measurements revealed that glimepiride (acid) and pioglitazone (ampholyte) were prone to supersaturation (*chaser*), as expected from their relatively high polar surface area and hydrogen-bonding capabilities. In contrast, sibutramine (base) was not expected to supersaturate and in fact it initially behaved as *non-chaser*, but later in the course of the titration it changed to a *chaser* behavior.

Shake-flask experiments suggest the formation of dimeric neutral aggregates of glimepiride and pioglitazone and points out the effect of buffering species in the solubility of sibutramine salts at acidic pH, particularly the salt formed with TFA, a constituent of the recommended minimalist universal buffer (MS-MUB). The pH variation during the equilibration step depends on the initial form of the sample (free acid/base or salt) and the solid form and solubility of the precipitate.

When aggregation reactions occur, as for glimepiride and pioglitazone, the intrinsic solubility calculated by the CheqSol method is similar to the apparent value determined by the shake-flask procedure. The potentiometric approach assumes a Henderson-Hasselbalch behavior, and thus the influence of additional aggregation equilibria is not considered. Fitting of the experimental shake-flask solubility-pH data to the appropriate model allows the determination of intrinsic solubilities (lower than the apparent ones) and aggregation numbers and constants.

Acknowledgements

This work was supported by the Ministry of Science, Innovation and Universities of Spain (project CTQ2017-88179-P AEI/FEDER, UE).

Conflict of interest statement

The authors declare no conflict of interest.

TABLES

Table 1. Comparison between shake-flask and CheqSol methods.

	Shake-flask method	CheqSol method
Accuracy	- Gold standard.	- Good correlation with SF.
Solubility measurement	- Thermodynamic (intrinsic solubility).	- Thermodynamic and kinetic (extent and duration of supersaturation).
Sample type	- All.	- Restricted to acid-base compounds.
pH profile	- Measurements performed at different pH values (including solubility of free species and salts, and aggregation reactions).	- Requires accurate measurement of pK_a and Henderson-Hasselbalch solubility behavior.
Sample consumption	- Large (depending on solubility).	- Lower in comparison to SF.
Laboratory equipment	- Inexpensive apparatus (with the exception, perhaps, of centrifuge for phase separation and instrument for quantification).	- Commercial titrator (SiriusT3, inForm, µDISS Profiler…).
Throughput	- Not suitable for screening. Labor intensive and time consuming.	- Low-throughput. Automated.
Solid identification	- Sufficient solid can be easily collected for PXRD and identified	- Changes in solubility can be observed in long-term analysis

Table 2. Calculated* molecular properties of the studied drugs.

Compound	H Acceptors	H Donors	Molecular Weight	log *P*	Freely Rotatable Bonds	Polar Surface Area (Å^2)
Glimepiride	9	3	490.62	3.4	6	133.0
Pioglitazone	5	1	356.44	3.5	7	93.6
Sibutramine	1	0	279.85	5.5	5	3.2

*Advanced Chemistry Development (ACD/Labs) Software V11.02 embedded in SciFinder Scholar.

Table 3. Potentiometrically determined acidity constants, intrinsic solubilities (S_0), supersaturation ratios (R_s) and times (t_{sat}) of the studied drugs (25 ºC and 0.15 M KCl ionic strength).

Compound	pK_a	Thermodynamic solubility: log S_0 (M)		Kinetic solubility	
		This work	Literature	R_s	t_{sat} (min)
Glimepiride	5.41 ± 0.06	-6.31 ± 0.12	-6.44[(a)]	124 ± 23	6 ± 1
Pioglitazone	5.67 ± 0.09; 6.60 ± 0.09	-5.81 ± 0.24	-6.16[(b)]	10 ± 2	7 ± 2
Sibutramine	8.74 ± 0.12	-5.33 ± 0.13	-	-	-

[(a)] (Narasimham and Barhate, 2011); [(b)](Schönherr et al., 2015).

Table 4. Glimepiride shake-flask intrinsic solubility values (25 ºC, log *S* in mol L^{-1}) found in the literature and determined in the present work. Measured solubility values in acidic solutions (pH < 6) are labeled as log S_0^{App}. These increased apparent solubility values are consistent with the formation of dimeric neutral aggregates, indicated by log K_2^{H2A2}.

$\log S_0$	$\log S_0^{App}$	$\log K_2^{H_2A_2}$	Comments
-7.14 ± 0.02	-6.63	7.18 ± 0.21	This work
-6.76 ± 0.07	-4.72	8.49 ± 0.09	pH 2.0-9.5; 0.05 M glycine; centrifuged, then filtered[(a)]
-7.21 ± 0.03	-5.47	8.65 ± 0.06	pH 4.5-8.2, 0.2 M phosphate; filtered[(b)]
-7.29			pH 6.5 (*I*=0.15M)[(c)], 37 ºC value corr. to 25 ºC[(d)]
-7.83 ± 0.10			pH ~ 3; centrifuged 3 times[(e)]; 21 ºC corr. to 25 ºC[(d)]

[(a)](Seedher and Kanojia, 2009); [(b)](Grbic et al., 2010); [(c)](Taupitz et al., 2013); [(d)](Avdeef, 2015); [(e)](Bergström et al., 2007).

Table 5. Pioglitazone shake-flask intrinsic solubility values (25ºC, log *S* in mol L^{-1}) found in the literature and determined in the present work.

$\log S_0$	Comments
-6.98 ± 0.04	This work
-6.63 ± 0.05	[(a)]
-6.86 ± 0.16	Hydrochloride salt; pH 2.0-9.5; 0.05 M glycine; centrifuged, then filtered[(b)]
-7.36	pH 2.4, 0.05 M phosphate, 3h incubation[(c)]; 37 ºC value corr. to 25 ºC[(d)]

[(a)](Sugita et al., 2014); [(b)](Seedher and Kanojia, 2009); [(c)](Tanaka et al., 2017); [(d)](Avdeef, 2015)

FIGURES

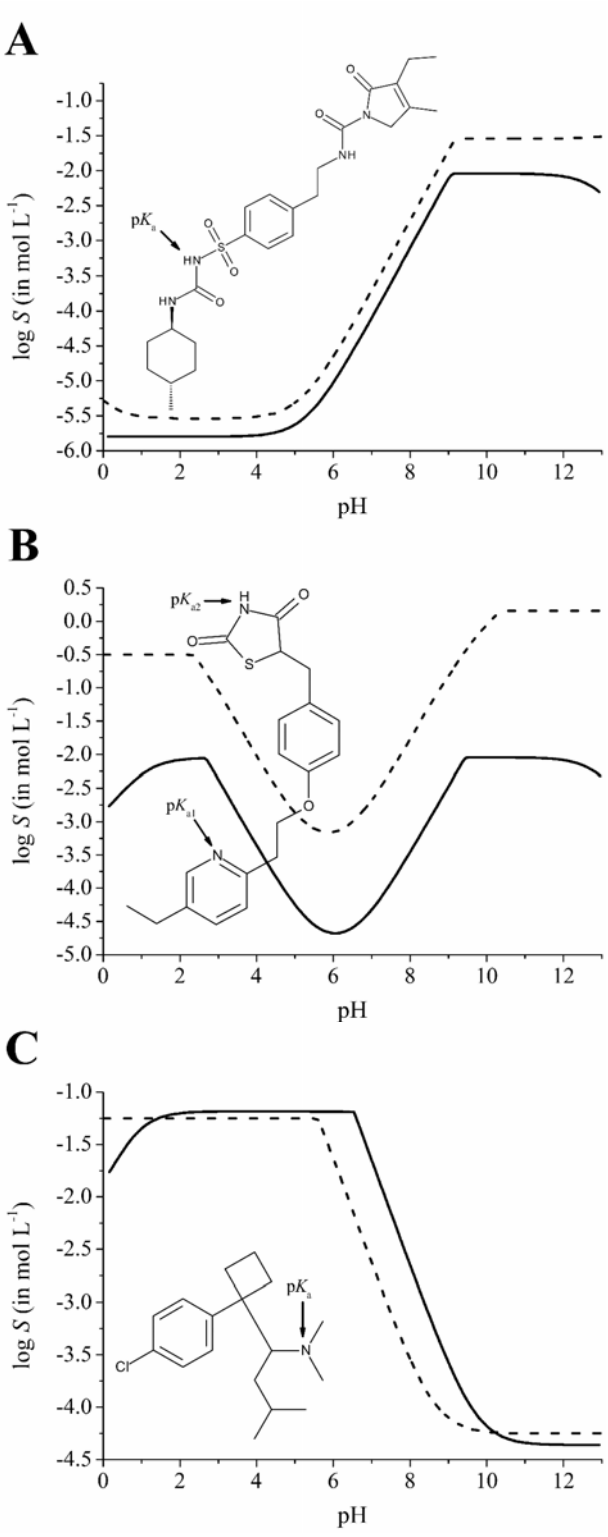

Figure 1. Predicted solubility-pH profiles for glimepiride (acid) (A), pioglitazone (ampholyte) (B), and sibutramine (base) (C) by means of ACD/Labs GALAS (dashed lines) and *p*-DISOL-X software (solid lines). The latter profile was calculated for a solution containing 0.15 M NaCl and assuming that the salt solubility of the drug can be estimated by the "sdiff 3-4" approximation (Avdeef, 2008; Avdeef et al., 2000).

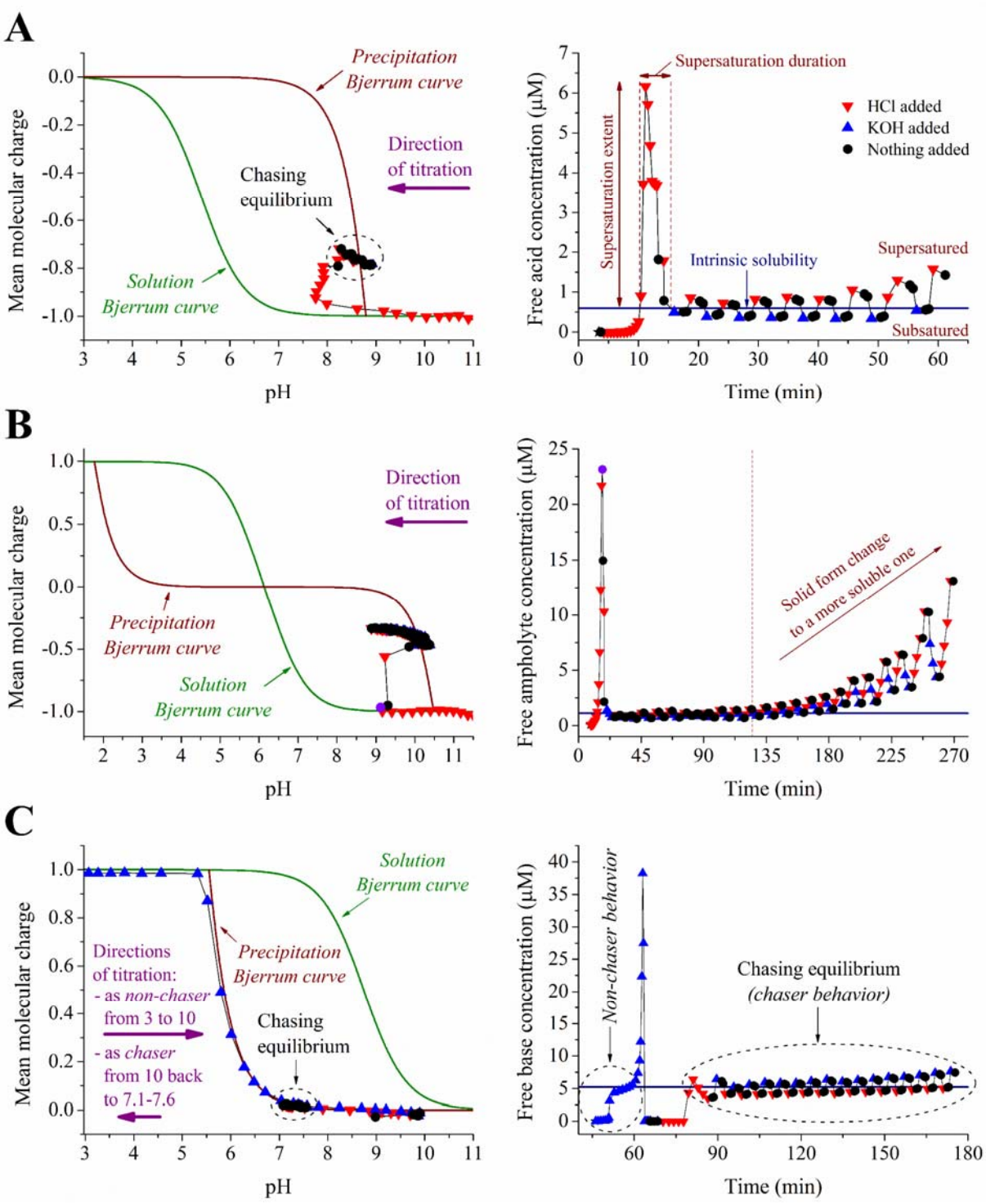

Figure 2. Mean molecular charge plots (*Bjerrum curves* and experimental data points, left panels) and neutral species concentration-time profiles (right panels) from CheqSol solubility measurements for glimepiride (A), pioglitazone (B), and sibutramine (C).

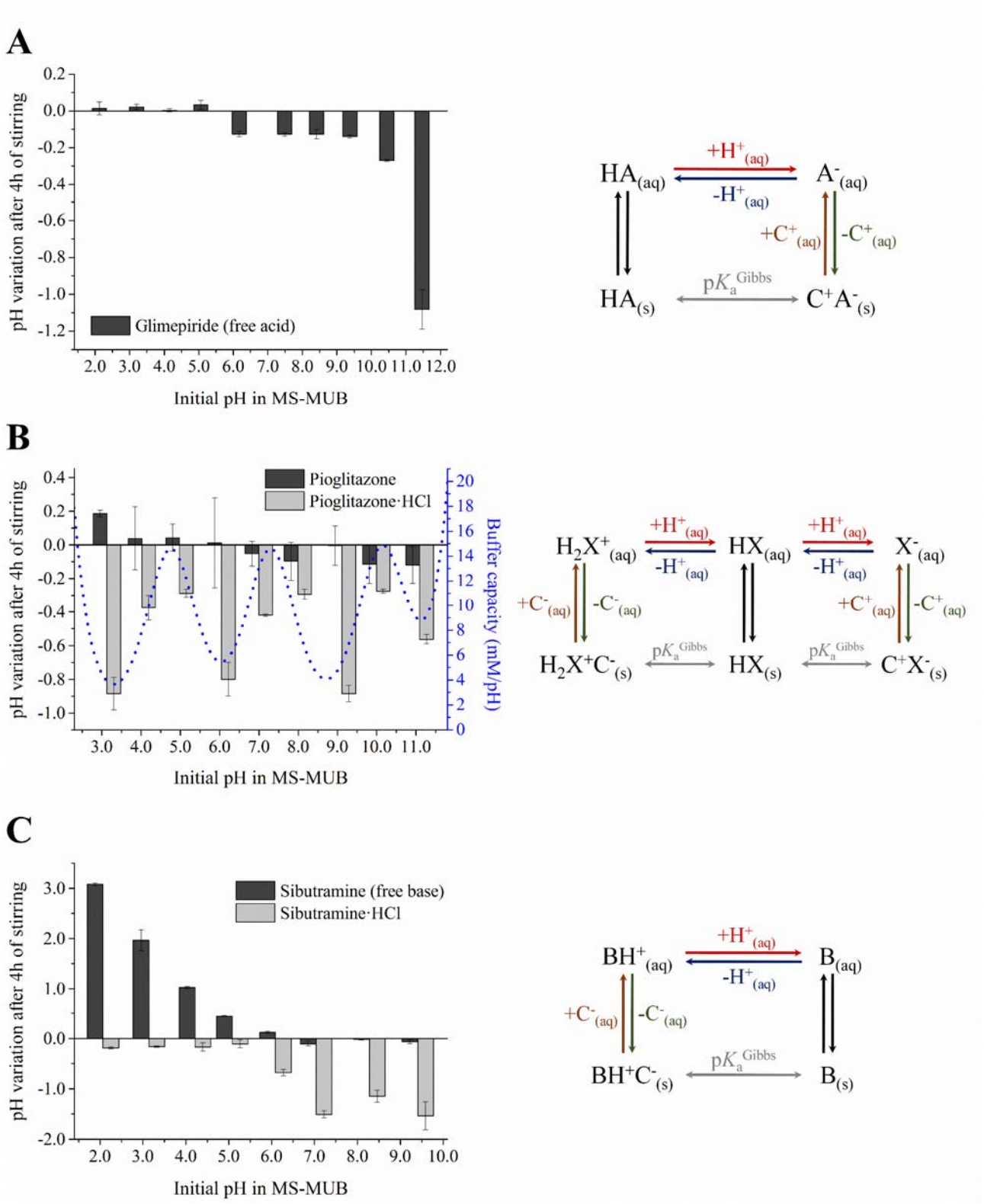

Figure 3. pH variation in the shake-flask method after 4h of stirring in relation to the initial aqueous buffer for glimepiride (A), pioglitazone (B), and sibutramine (C). The starting solid (free species or salt) is presented in the figure, together with the buffer capacity variation of the buffer (MS-MUB, dotted line) along the studied pH range (B) and a scheme of the different species in equilibria.

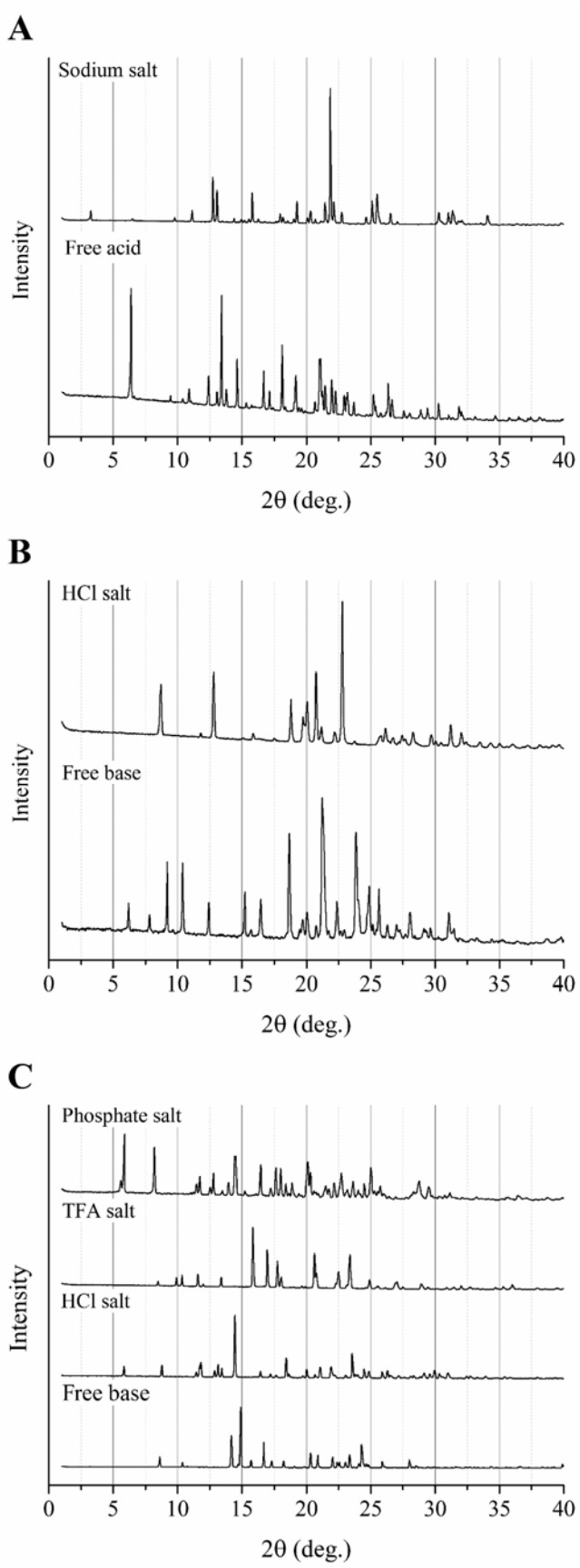

Figure 4. Diffractrograms of different forms of glimepiride (A), pioglitazone (B), and sibutramine (C) in the course of shake-flask experiments.

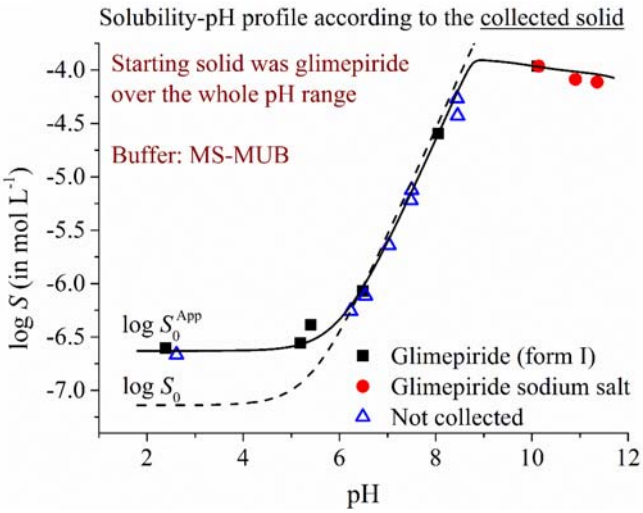

Figure 5. Shake-flask solubility-pH profile of glimepiride according to the collected solid. Dashed line represents the Henderson-Hasselbalch theoretical fitting.

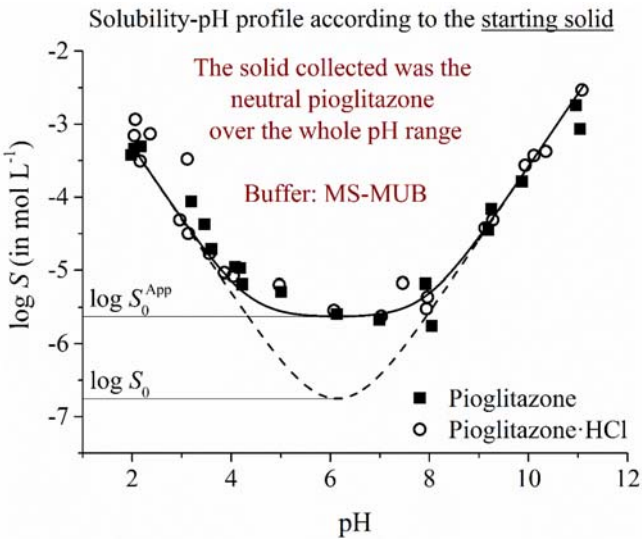

Figure 6. Shake-flask solubility-pH profile of pioglitazone according to the starting solid. Solid line show the fitted curve to Eq. (3). Dashed line represents the Henderson-Hasselbalch theoretical fitting.

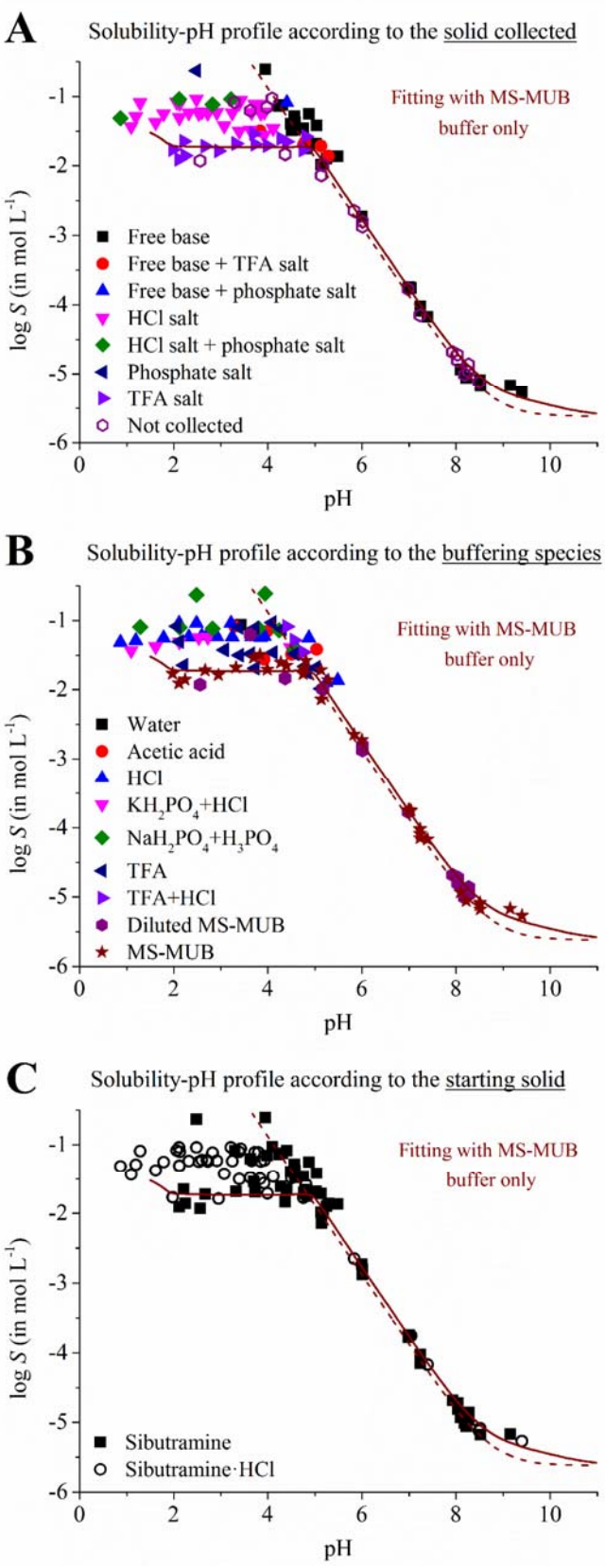

Figure 7. Shake-flask solubility-pH profiles of sibutramine showing the effect of the starting solid and the buffering species on the finally collected solid. Dashed line represents the Henderson-Hasselbalch theoretical fitting.

REFERENCES

ACD/Labs. Advanced Chemistry Development, Inc. Toronto, ON, Canada, 2019.

Amidon, G.L., Lennernäs, H., Shah, V.P., Crison, J.R., 1995. A Theoretical Basis for a Biopharmaceutic Drug Classification: The Correlation of in Vitro Drug Product Dissolution and in Vivo Bioavailability. Pharm. Res. 12, 413–420. https://doi.org/10.1023/A:1016212804288

Avdeef, A., 2018. Cocrystal solubility-pH and drug solubilization capacity of sodium dodecyl sulfate - Mass action model for data analysis and simulation to improve design of experiments. ADMET DMPK 6, 105–139. https://doi.org/10.5599/admet.505

Avdeef, A., 2015. Solubility Temperature Dependence Predicted from 2D Structure. ADMET DMPK 3, 298–344. https://doi.org/10.5599/admet.3.4.259

Avdeef, A., 2012. Absorption and drug development, Second. ed, Absorption and Drug Development: Solubility, Permeability, and Charge State. John Wiley & Sons, Inc., Hoboken, NJ, USA. https://doi.org/10.1002/9781118286067

Avdeef, A., 2008. Drug Ionization and Physicochemical Profiling, in: Mannhold, R. (Ed.), Molecular Drug Properties: Measurement and Prediction, Methods and Principles in Medicinal Chemistry. pp. 53–83. https://doi.org/10.1002/9783527621286.ch3

Avdeef, A., 2007. Solubility of sparingly-soluble ionizable drugs. Adv. Drug Deliv. Rev. 59, 568–590. https://doi.org/10.1016/j.addr.2007.05.008

Avdeef, A., 1998. pH-metric solubility. 1. Solubility-pH profiles from Bjerrum plots. Gibbs buffer and pK(a) in the solid state. Pharm. Pharmacol. Commun. 4, 165–178. https://doi.org/10.1111/j.2042-7158.1998.tb00328.x

Avdeef, A., Berger, C.M., Brownell, C., 2000. pH-metric solubility. 2: Correlation between the acid-base titration and the saturation shake-flask solubility-pH methods. Pharm. Res. 17, 85–89. https://doi.org/10.1023/A:1007526826979

Avdeef, A., Comer, J.E.A., Thomson, S.J., 1993. pH-Metric log *P*. 3. Glass electrode calibration in methanol-water, applied to pK_a determination of water-insoluble substances. Anal. Chem. 65, 42–49. https://doi.org/10.1021/ac00049a010

Avdeef, A., Fuguet, E., Llinàs, A., Ràfols, C., Bosch, E., Völgyi, G., Verbić, T., Boldyreva, E., Takács-Novák, K., 2016. Equilibrium solubility measurement of ionizable drugs – consensus recommendations for improving data quality. ADMET DMPK 4, 117–178. https://doi.org/10.5599/admet.4.2.292

Bergström, C.A.S., Wassvik, C.M., Johansson, K., Hubatsch, I., 2007. Poorly Soluble Marketed Drugs Display Solvation Limited Solubility. J. Med. Chem. 50, 5858–5862. https://doi.org/10.1021/jm0706416

Bonfilio, R., Pires, S.A., Ferreira, L.M.B., de Almeida, A.E., Doriguetto, A.C., de Araújo, M.B., Salgado, H.R.N., 2012. A Discriminating Dissolution Method for Glimepiride Polymorphs. J. Pharm. Sci. 101, 794–804. https://doi.org/10.1002/jps.22799

Box, K., Comer, J.E., Gravestock, T., Stuart, M., 2009. New ideas about the solubility of drugs. Chem. Biodivers. 6, 1767–1788. https://doi.org/10.1002/cbdv.200900164

Box, K.J., Völgyi, G., Baka, E., Stuart, M., Takács-Novák, K., Comer, J.E.A., 2006. Equilibrium versus kinetic measurements of aqueous solubility, and the ability of compounds to supersaturate in solution—a validation study. J. Pharm. Sci. 95, 1298–1307. https://doi.org/10.1002/jps.20613

Di, L., Fish, P. V., Mano, T., 2012. Bridging solubility between drug discovery and development. Drug Discov. Today 17, 486–495. https://doi.org/10.1016/j.drudis.2011.11.007

EMA, 2018. ICH guideline M9 on biopharmaceutics classification system based biowaivers - Step 2b - First version [WWW Document]. URL https://www.ema.europa.eu/en/documents/scientific-guideline/ich-m9-biopharmaceutics-classification-system-based-biowaivers-step-2b-first-version_en.pdf (accessed 9.23.19).

Endo, T., Iwata, M., Nagase, H., Shiro, M., Ueda, H., 2003. Polymorphism of glimepiride: crystallographic study, thermal transitions behavior and dissolution study. STP Pharma Sci. 13, 281–286.

FDA, 2017. Waiver of In Vivo Bioavailability and Bioequivalence Studies for Immediate-Release Solid Oral Dosage Forms Based on a Biopharmaceutics Classification System [WWW Document]. URL https://www.fda.gov/media/70963/download (accessed 9.23.19).

Gebauer, D., Kellermeier, M., Gale, J.D., Bergström, L., Cölfen, H., 2014. Pre-nucleation clusters as solute precursors in crystallisation. Chem. Soc. Rev. 43, 2348–2371. https://doi.org/10.1039/C3CS60451A

Grbic, S., Parojcic, J., Malenovic, A., Djuric, Z., Maksimovic, M., 2010. A Contribution to the Glimepiride Dissociation Constant Determination. J. Chem. Eng. Data 55, 1368–1371. https://doi.org/10.1021/je900546z

Grell, W., Hurnaus, R., Griss, G., Sauter, R., Rupprecht, E., Mark, M., Luger, P., Nar, H., Wittneben, H., Mueller, P., 1998. Repaglinide and Related Hypoglycemic Benzoic Acid Derivatives. J. Med. Chem. 41, 5219–5246. https://doi.org/10.1021/jm9810349

Gryl, M., Krawczuk-Pantula, A., Stadnicka, K., 2011. Charge-density analysis in polymorphs of urea–barbituric acid co-crystals. Acta Crystallogr. Sect. B Struct. Sci. 67, 144–154. https://doi.org/10.1107/S0108768111002412

in-ADME Research. New York City, USA, 2019.

Irwin, J.J., Duan, D., Torosyan, H., Doak, A.K., Ziebart, K.T., Sterling, T., Tumanian, G., Shoichet,

B.K., 2015. An Aggregation Advisor for Ligand Discovery. J. Med. Chem. 58, 7076–7087. https://doi.org/10.1021/acs.jmedchem.5b01105

Iwata, M., Nagase, H., Endo, T., Ueda, H., 1997. Glimepiride. Acta Crystallogr. Sect. C Cryst. Struct. Commun. 53, 329–331. https://doi.org/10.1107/S0108270196002363

Marković, O.S., Pešić, M.P., Shah, A. V., Serajuddin, A.T.M., Verbić, T., Avdeef, A., 2019. Solubility-pH profile of desipramine hydrochloride in saline phosphate buffer: Enhanced solubility due to drug-buffer aggregates. Eur. J. Pharm. Sci. 133, 264–274. https://doi.org/10.1016/j.ejps.2019.03.014

Narasimham, L., Barhate, V.D., 2011. Kinetic and intrinsic solubility determination of some b-blockers and antidiabetics by potentiometry. J. Pharm. Res. 4, 532–536.

Schönherr, D., Wollatz, U., Haznar-Garbacz, D., Hanke, U., Box, K.J., Taylor, R., Ruiz, R., Beato, S., Becker, D., Weitschies, W., 2015. Characterisation of selected active agents regarding pK_a values, solubility concentrations and pH profiles by SiriusT3. Eur. J. Pharm. Biopharm. 92, 155–170. https://doi.org/10.1016/j.ejpb.2015.02.028

Seedher, N., Kanojia, M., 2009. Co-solvent solubilization of some poorly-soluble antidiabetic drugs. Pharm. Dev. Technol. 14, 185–192. https://doi.org/10.1080/10837450802498894

Seedher, N., Kanojia, M., 2008. Micellar Solubilization of Some Poorly Soluble Antidiabetic Drugs: A Technical Note. AAPS PharmSciTech 9, 431–436. https://doi.org/10.1208/s12249-008-9057-5

Shoghi, E., Fuguet, E., Bosch, E., Ràfols, C., 2013. Solubility-pH profiles of some acidic, basic and amphoteric drugs. Eur. J. Pharm. Sci. 48, 291–300. https://doi.org/10.1016/j.ejps.2012.10.028

Stuart, M., Box, K., 2005. Chasing equilibrium: Measuring the intrinsic solubility of weak acids and bases. Anal. Chem. 77, 983–990. https://doi.org/10.1021/ac048767n

Sugita, M., Kataoka, M., Sugihara, M., Takeuchi, S., Yamashita, S., 2014. Effect of Excipients on the Particle Size of Precipitated Pioglitazone in the Gastrointestinal Tract: Impact on Bioequivalence. AAPS J. 16, 1119–1127. https://doi.org/10.1208/s12248-014-9646-z

Tam, K.Y., Takács-Novák, K., 2001. Multi-wavelength spectrophotometric determination of acid dissociation constants: A validation study. Anal. Chim. Acta 434, 157–167. https://doi.org/10.1016/S0003-2670(01)00810-8

Tanaka, Y., Sugihara, M., Kawakami, A., Imai, S., Itou, T., Murase, H., Saiki, K., Kasaoka, S., Yoshikawa, H., 2017. In vivo analysis of supersaturation/precipitation/absorption behavior after oral administration of pioglitazone hydrochloride salt; determinant site of oral absorption. Eur. J. Pharm. Sci. 106, 431–438. https://doi.org/10.1016/j.ejps.2017.06.011

Taupitz, T., Dressman, J.B., Klein, S., 2013. New formulation approaches to improve solubility and drug release from fixed dose combinations: Case examples pioglitazone/glimepiride and

ezetimibe/simvastatin. Eur. J. Pharm. Biopharm. 84, 208–218. https://doi.org/10.1016/j.ejpb.2012.11.027

Tian, F., Zimmerman, A., 2017a. Method for preparing glimepiride α crystal form. Faming Zhuanli Shenqing. CN106866486A.

Tian, F., Zimmerman, A., 2017b. β Crystal form of glimepiride and preparation method thereof. Faming Zhuanli Shenqing. CN106883161A.

Tian, F., Zimmerman, A., 2017c. Method for preparing glimepiride δ crystal form. Faming Zhuanli Shenqing. CN106866485A.

Tian, F., Zimmerman, A., 2017d. Preparation of glimepiride crystal form ε. Faming Zhuanli Shenqing. CN106866487A.

Tian, F., Zimmerman, A., 2017e. Glimepiride γ crystal form and preparation method thereof. Faming Zhuanli Shenqing. CN106699631A.

Veseli, A., Žakelj, S., Kristl, A., 2019. A review of methods for solubility determination in biopharmaceutical drug characterization. Drug Dev. Ind. Pharm. 45, 1717–1724. https://doi.org/10.1080/03639045.2019.1665062

Völgyi, G., Marosi, A., Takács-Novák, K., Avdeef, A., 2013. Salt Solubility Products of Diprenorphine Hydrochloride, Codeine and Lidocaine Hydrochlorides and Phosphates – Novel Method of Data Analysis Not Dependent on Explicit Solubility Equations. ADMET DMPK 1, 48–62. https://doi.org/10.5599/admet.1.4.24

APPENDIX

Table A.1. Measured solubilities at different pH values by the shake-flask method using MS-MUB as buffering system (25 ºC).

Compound	pH[a,b]	log *S* (M)[b]	Solid in equilibrium[c]
Glimepiride	2.39	-6.60	Form I
	2.61	-6.60	-
	5.19	-6.56	Form I
	5.40	-6.39	Form I
	6.23±0.05	-6.26±0.18	-
	6.49±0.02	-6.07±0.15	Form I
	6.54±0.04	-6.11±0.11	-
	7.03±0.04	-5.64±0.04	-
	7.49±0.03	-5.22±0.03	-
	7.50±0.03	-5.12±0.01	-
	8.06±0.06	-4.59±0.06	Form I
	8.45±0.04	-4.27±0.04	-
	8.46±0.08	-4.43±0.23	-
	10.02±0.01	-3.97±0.02	Form I
	10.14±0.02	-3.96±0.01	Form I + unidentified phase
	10.90±0.02	-4.09±0.04	Form I + unidentified phase
	11.35±0.06	-4.11±0.02	Form I + unidentified phase
Sibutramine	2.12	--1.91	TFA salt
	2.24	-1.86	TFA salt
	3.33	-1.68	TFA salt
	3.70±0.09	-1.54±0.02	TFA salt
	4.28±0.03	-1.61±0.10	TFA salt
	4.41	-1.64	TFA salt
	4.52±0.02	-1.07±0.08	Free base and unidentified phase
	4.76±0.20	-1.69±0.05	Freebase + TFA salt
	5.12±0.01	-1.71±0.03	Freebase + TFA salt
	5.14±0.07	-2.13±0.1	-
	5.29±0.02	-1.87±0.03	Freebase + TFA salt
	6.00±0.01	-2.72±0.05	Freebase
	6.99±0.03	-3.75±0.03	Freebase
	7.24±0.06	-4.09±0.05	Freebase
	8.01±0.11	-4.93±0.11	Freebase
	8.22±0.01	-5.06±0.03	Freebase
	8.52±0.12	-5.18±0.16	Freebase
Sibutramine HCl	1.98±0.08	-1.76±0.09	TFA salt
	2.95±0.08	-1.78±0.02	TFA salt
	3.83±0.03	-1.50±0.09	Freebase + TFA salt
	3.99±0.07	-1.71±0.12	TFA salt
	4.75	-1.77	TFA salt
	4.81±0.04	-1.58±0.08	TFA salt

	5.84±0.04	-2.65±0.03	-
	7.04±0.07	-3.76±0.04	Freebase
	7.39±0.09	-4.17±0.11	Freebase
	8.49±0.09	-5.12±0.27	-
	8.51±0.12	-5.08±0.11	Freebase
	9.40±0.12	-5.27±0.15	Freebase
Pioglitazone	1.98	-3.43	Pioglitazone
	2.03	-3.34	Pioglitazone
	2.18	-3.31	Pioglitazone
	3.19±0.10	-4.06±0.09	Pioglitazone
	3.46±0.01	-4.37±0.04	-
	3.60	-4.71	-
	4.08	-4.96	Pioglitazone
	4.18±0.01	-4.97±0.03	-
	4.22±0.01	-5.19±0.01	Pioglitazone
	5.06±0.01	-5.62±0.04	-
	5.01±0.02	-5.29±0.05	-
	6.13±0.01	-5.59±0.07	-
	7.00±0.04	-5.67±0.22	-
	7.92±0.02	-5.18±0.07	Pioglitazone
	8.04±0.01	-5.76±0.02	-
	9.19±0.01	-4.45±0.02	-
	9.25	-4.16	Pioglitazone
	9.87±0.01	-3.79±0.04	Pioglitazone
	10.96±0.05	-2.74±0.06	Pioglitazone
	11.04±0.02	-3.07±0.02	-
PioglitazoneHCl	2.04	-3.16	-
	2.06	-2.94	Pioglitazone
	2.16±0.03	-3.51±0.03	-
	2.36	-3.13	-
	2.96	-4.31	-
	3.11	-3.48	-
	3.12±0.08	-4.50±0.14	-
	3.56	-4.77	-
	3.86±0.11	-5.03±0.09	-
	4.04±0.07	-5.08±0.07	Pioglitazone
	4.97±0.03	-5.20±0.12	-
	6.07±0.04	-5.54±0.08	-
	7.04±0.05	-5.62±0.14	-
	7.46±0.01	-5.17±0.07	-
	7.94±0.01	-5.52±0.05	-
	7.94±0.07	-5.36±0.06	-
	9.11±0.04	-4.42±0.04	-
	9.28±0.09	-4.31±0.11	-
	9.93±0.03	-3.56±0.05	-

9.99±0.01	-3.43±0.02	-
10.35±0.01	-3.37±0.06	-
11.08±0.06	-2.53±0.01	-

[a] pH measured at the end of the sedimentation step, just before the phase separation by centrifugation.

[b] Replicate measurements at similar pH values (standard deviations ≤ 0.1) are reported as their average log S ± standard deviation. On the contrary, individual replicates are presented instead.

[c] Identification by PXRD.

Table A.2. PXRD peak lists (position, 2θ (°)) of glimepiride crystal forms reported in published patents (α, β, γ, δ and ε), simulated peak lists from crystal structures (forms I and II) and the new sodium salt phase characterized in this work.

Glimepiride polymorphs reported							New phase
α[1]	β[2]	γ[3]	δ[4]	ε[5]	I[6]	II[7]	sodium salt
6.916					6.480	7.950	3.259
7.200					10.970	10.527	9.785
8.748		9.729		9.478	12.484	12.057	11.153
10.378	10.895	10.033		10.110	13.140	12.503	12.767
11.166	11.515	10.667	11.521	10.869	13.495	13.874	13.084
14.017	12.316	12.995	14.231	11.447	13.863	14.389	14.399
15.654	14.534	13.408	15.061	12.390	14.707	15.437	14.962
17.107	14.923	17.854	16.529	13.044	16.756	15.934	15.216
17.330	15.287	19.537	18.775	14.414	17.222	16.119	15.553
18.349	16.277		20.536	15.694	18.206	16.967	15.828
19.152	16.549		22.156	18.650	19.239	18.280	16.287
21.103	17.645		30.579	18.984	20.713	18.621	17.998
23.222	19.019		31.025	19.334	21.101	19.545	18.573
23.662	21.952		31.708	21.828	21.348	19.823	19.052
24.038	22.295			22.291	21.530	20.304	20.112
24.332	23.539			22.805	22.030	21.234	20.354
26.197	25.103			23.637	22.320	21.437	21.132
27.055	26.261			24.693	22.994	21.535	21.900
27.888	31.841			25.725	23.189	22.063	22.183
28.178	33.044			27.188	23.332	22.849	22.780
28.634	33.955			31.680	23.739	23.246	24.677
29.085				34.046	25.295	23.781	25.156
30.534					25.847	23.921	25.531
33.804					26.426	24.014	26.581
34.546					26.717	24.283	27.109
35.048					28.945	24.384	31.071
					29.510	25.158	31.397
					30.322	27.946	31.510
					31.939	29.454	34.087

Table A.3. PXRD peak list of the TFA sibutramine salt phase characterized in this work.

Sibutramine TFA salt		Sibutramine phosphate salt	
Position 2θ (º)	Relative intensity (%)	Position 2θ (º)	Relative intensity (%)
8.479	8.4	5.593	20.5
9.917	14.1	5.855	100.0
10.353	18.1	8.202	78.6
11.588	21.8	11.471	17.3
11.993	3.9	11.727	30.3
13.386	16.0	12.789	37.6
15.859	100.0	13.957	20.9
16.977	63.8	14.431	64.7
17.759	44.6	14.550	61.2
18.048	17.6	16.453	52.7
20.631	56.0	17.639	48.2
20.806	22.5	18.014	46.9
22.284	8.4	18.413	20.9
22.500	28.1	18.887	22.9
23.127	5.2	20.103	57.2
23.391	55.6	20.318	40.6
24.918	15.6	22.160	23.5
26.928	9.8	22.734	40.2
27.050	11.9	23.634	26.1
28.890	8.6	24.510	21.8
32.018	6.1	25.014	50.6
35.989	8.3	25.745	19.5
		28.775	28.0
		29.540	18.3

Characterization of the solids

Figure S.1: DSC of glimepiride sodium salt

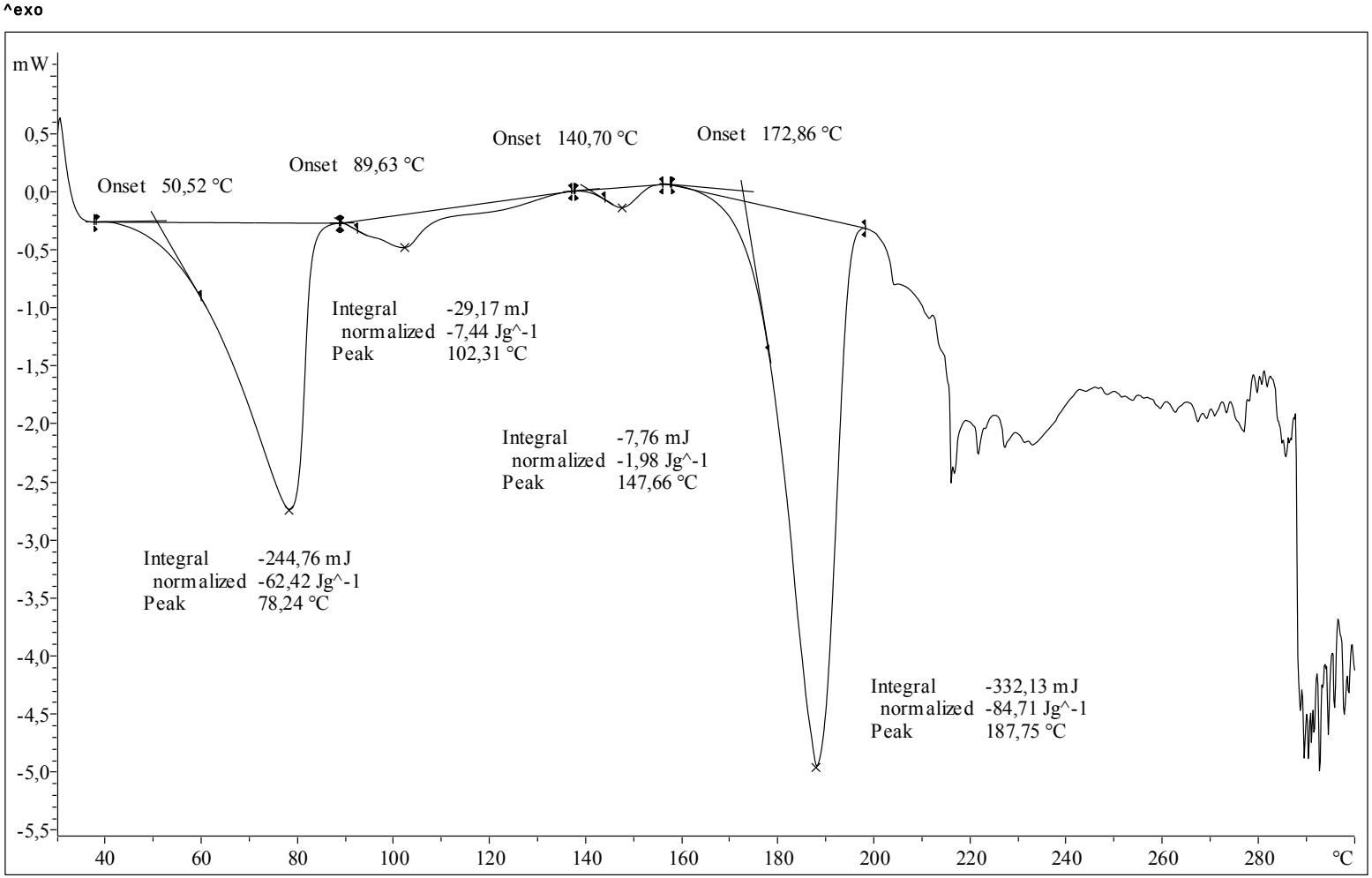

Figure S.2: TGA of glimepiride sodium salt

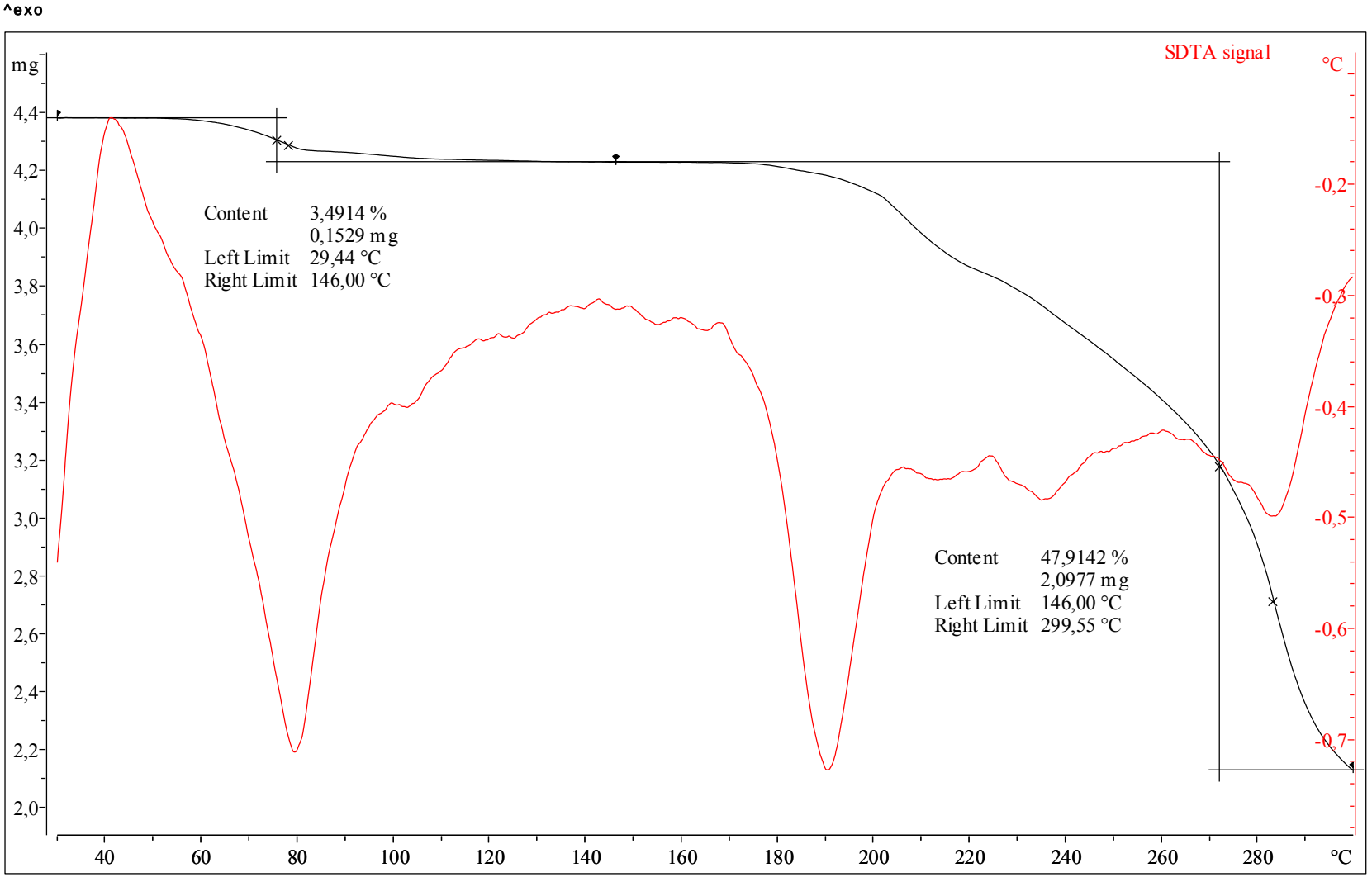

Figure S.3: PXRD of glimepiride sodium salt

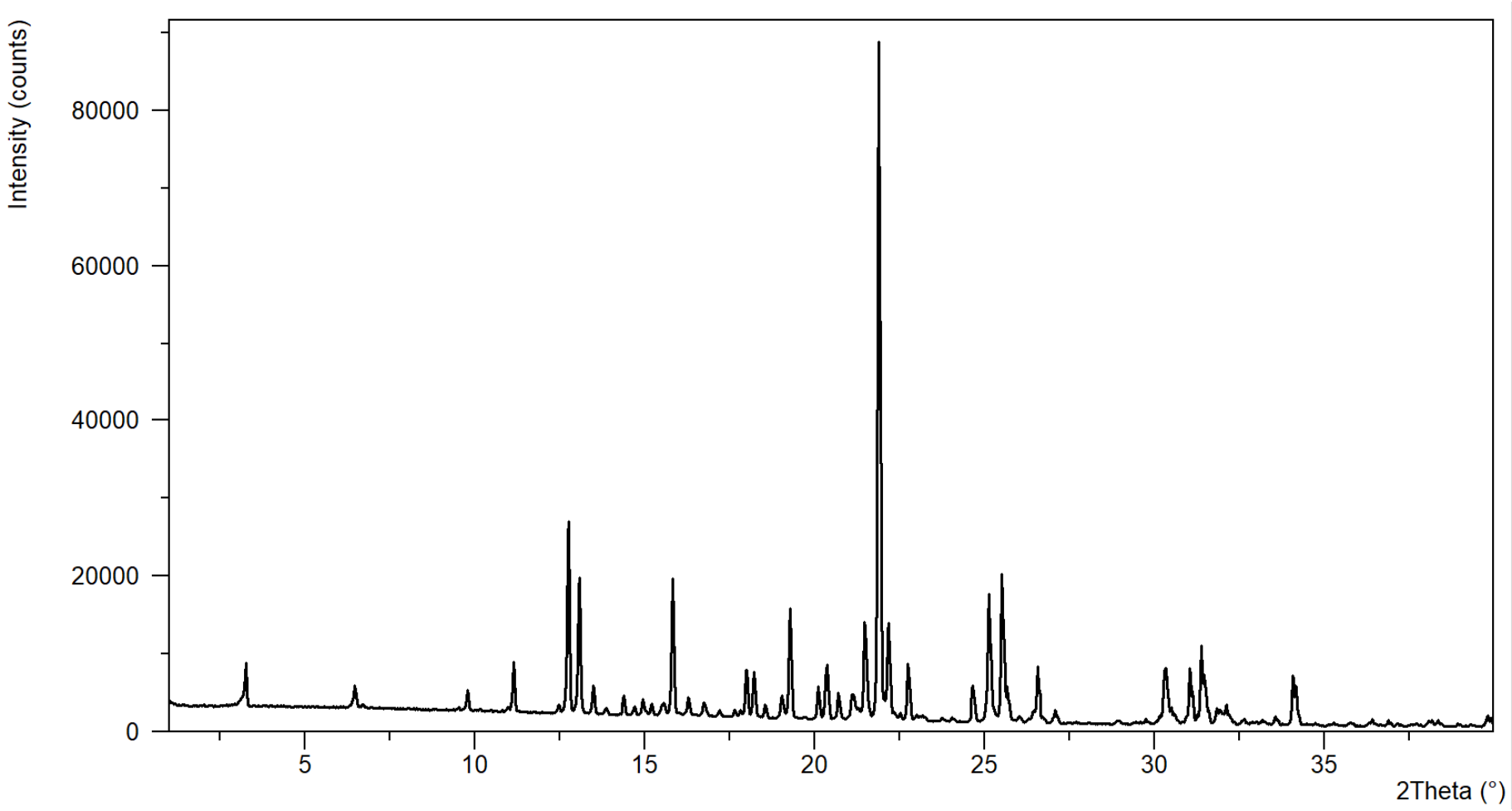

Figure S.4: DSC of sibutramine-TFA salt

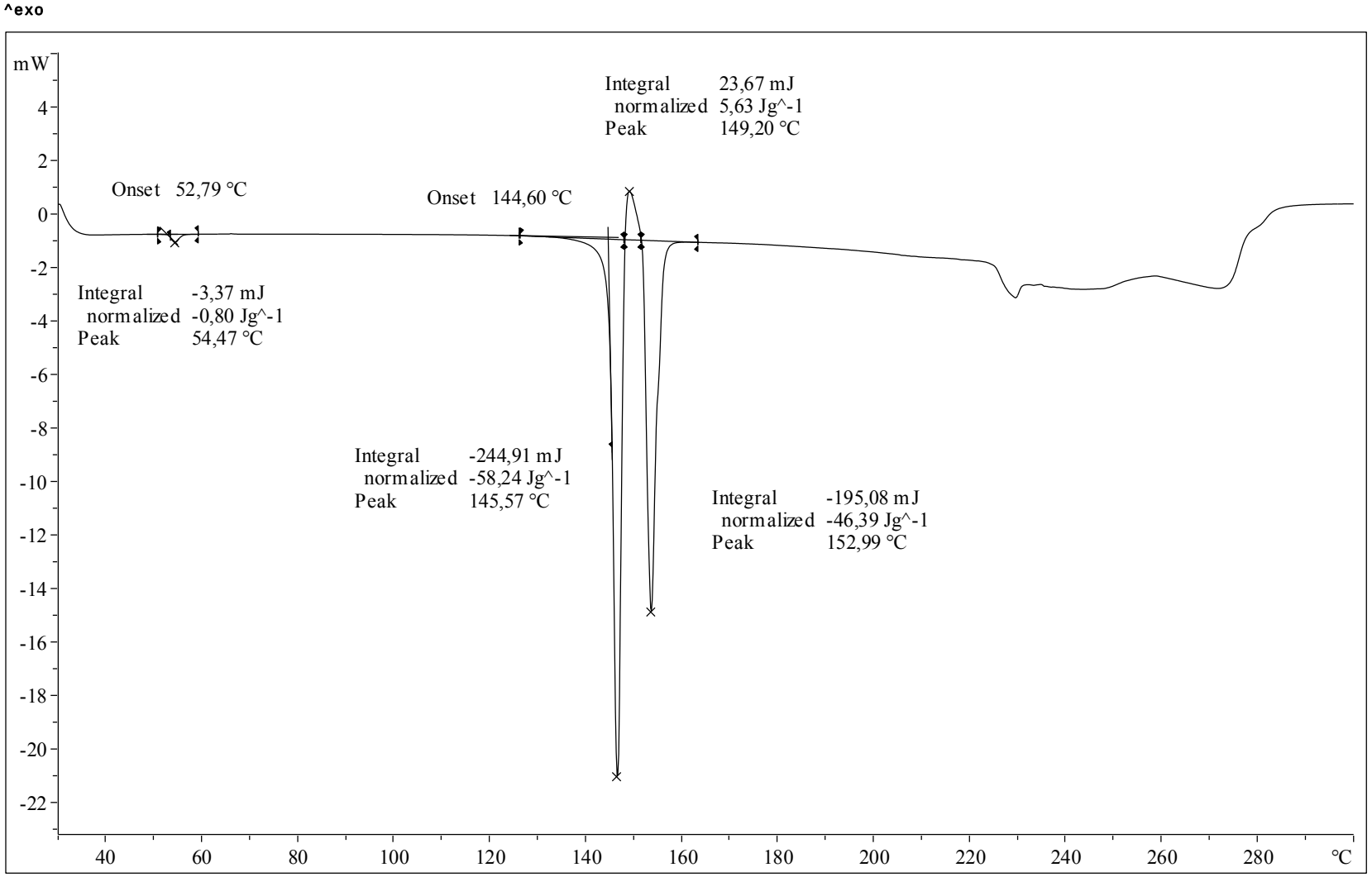

Figure S.5: TGA of sibutramine-TFA salt

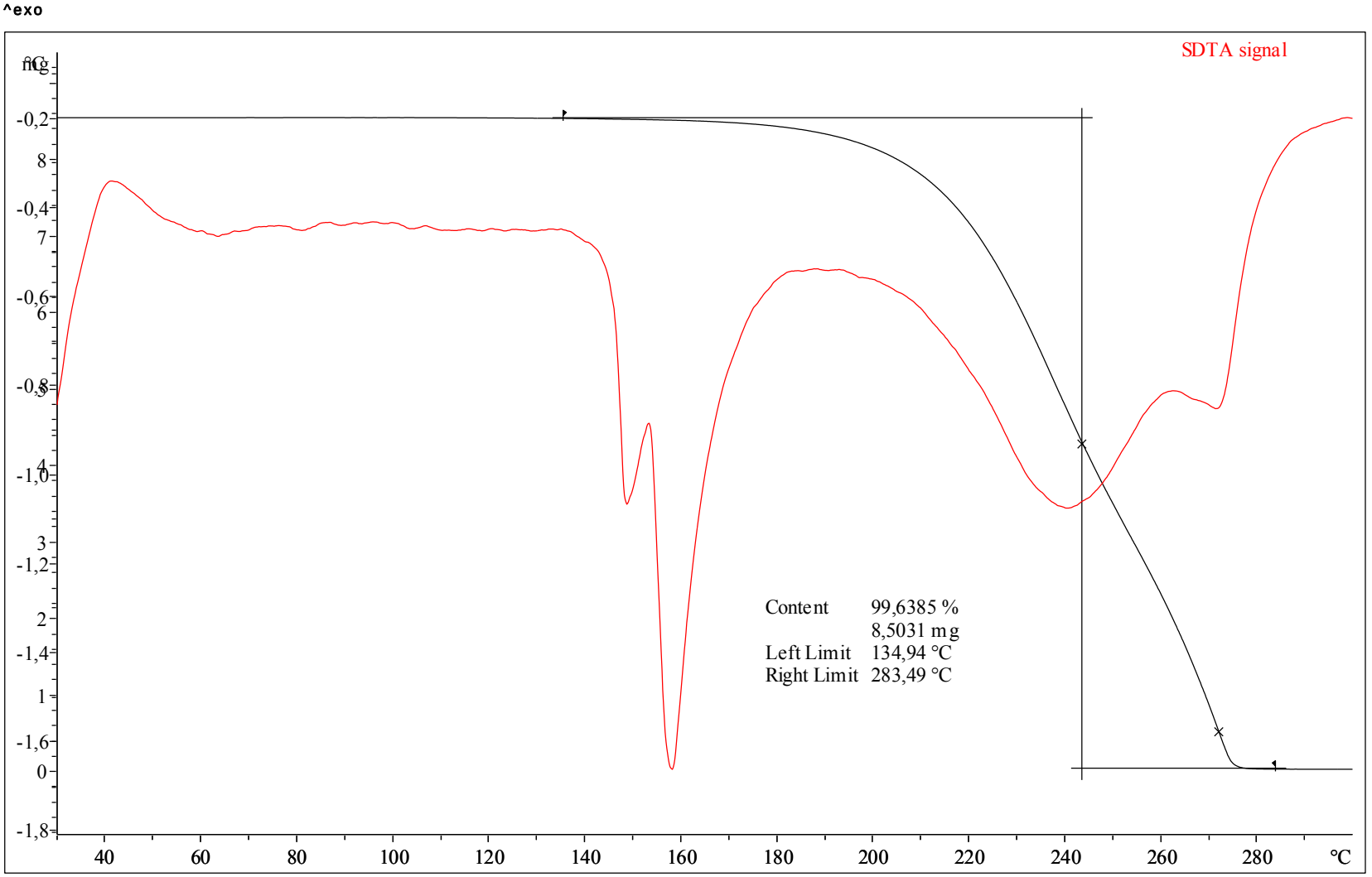

The powder diffractogram was indexed and the lattice parameters were refined by means of the LeBail method, program Dicvol04[8], and the space group was determined from the systematic absences. The cell volume is compatible with 1 molecule of sibutramine and 1 molecule of trifluoroacetic acid in the asymmetric unit, Z=4, (assuming a density value of 1.3).

Figure S6: The XRPD diagram of Form SIBU-TFA has been indexed with the following monoclinic cell: a=17.439(2) Å, b=10.434(1) Å, c=11.422(1) Å, β= 102.230(5)º, V=2031.1(4) Å^3 (Figures of Merit: M= 27, F= 70), according to systematic absences $P2_1/n$ or $P2_1/c$ space groups are compatible with the cell

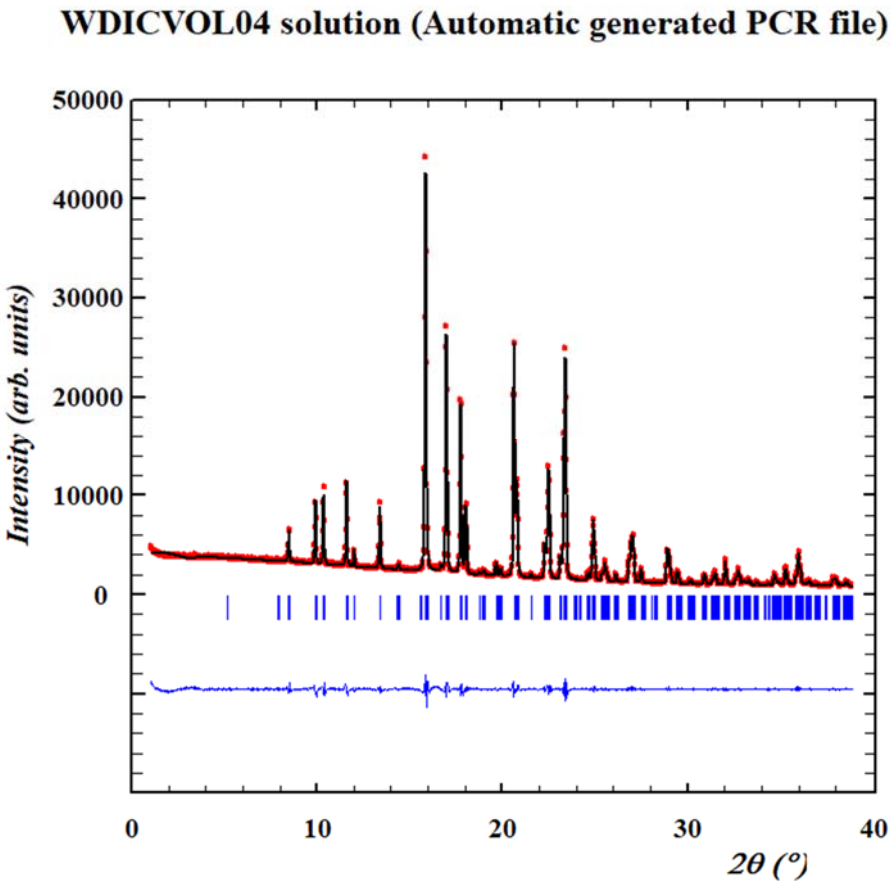

The powder diffractogram was indexed and the lattice parameters were refined by means of the LeBail method, program Dicvol04[8], and the space group was determined from the systematic absences. The cell volume is compatible with 1 molecule of sibutramine and 1 molecule of phosphoric acid in the asymmetric unit, Z=4, (assuming a density value of 1.2).

Figure S7: The XRPD diagram of Form SIBU-phosphate has been indexed with the following triclinic cell: a=30.920(6) Å, b=19.905(3) Å, c=9.342(1) Å, α= 49.193(9)º, β= 134.517(8)º, γ= 146.692(6)º, V=2217.9(6) Å^3 (Figures of Merit: M= 45, F= 152).

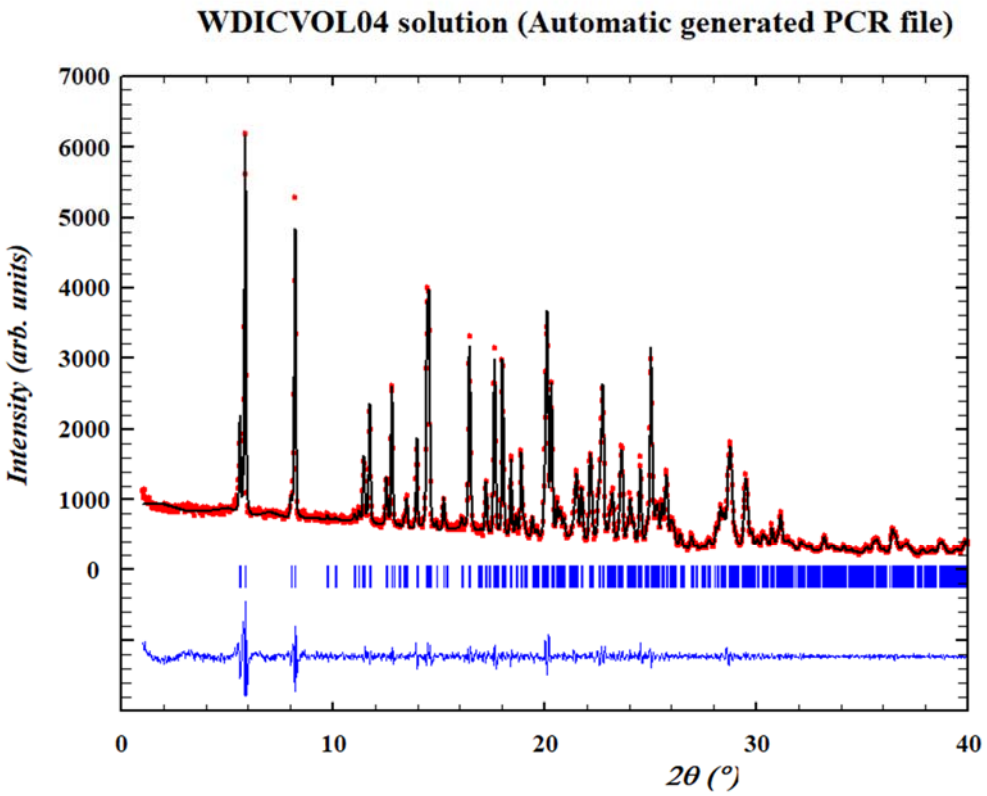

References:

[1] F. Tian, A. Zimmerman, Method for preparing glimepiride α crystal form, CN106866486A, 2017.
[2] F. Tian, A. Zimmerman, β Crystal form of glimepiride and preparation method thereof, CN106883161A, 2017.
[3] F. Tian, A. Zimmerman, Glimepiride γ crystal form and preparation method thereof, CN106699631A, 2017.
[4] F. Tian, A. Zimmerman, Method for preparing glimepiride δ crystal form, CN106866485A, 2017.
[5] F. Tian, A. Zimmerman, Preparation of glimepiride crystal form ε, CN106866487A, 2017.
[6] W. Grell, R. Hurnaus, G. Griss, R. Sauter, E. Rupprecht, M. Mark, P. Luger, H. Nar, H. Wittneben, P. Mueller, Repaglinide and Related Hypoglycemic Benzoic Acid Derivatives., J. Med. Chem. 41 (1998) 5219–5246. doi:10.1021/jm9810349. (CCDC code: TOHBUN01)
[7] M. Iwata, H. Nagase, T. Endo, H. Ueda, Glimepiride, Acta Crystallogr. Sect. C Cryst. Struct. Commun. 53 (1997) 329–331. doi:10.1107/S0108270196002363. (CCDC code: TOHBUN02)
[8] A. Boultif, D. Louër, Indexing of powder diffraction patterns for low-symmetry lattices by the successive dichotomy method, J. Appl. Crystallogr. 24 (1991) 987–993. doi:10.1107/S0021889891006441